Short-chain Fatty Acid Acetate Stimulates Adipogenesis and Mitochondrial Biogenesis via GPR43 in Brown Adipocytes

Jiamiao Hu[1], Ioannis Kyrou[2,7], Bee K Tan[1,2,3], Georgios K Dimitriadis[1,2], Manjunath Ramanjaneya[4], Gyanendra Tripathi[1], Vanlata Patel[1], Sean James[5], Mohamed Kawan[1], Jing Chen[1,6*], Harpal S Randeva[1,2,7*]

[*]Joint senior and corresponding authors, contribute equally to the manuscript.

[1]Translational & Experimental Medicine, Division of Biomedical Sciences, Warwick Medical School, University of Warwick, CV4 7AL, Coventry, UK;

[2]WISDEM, University Hospitals Coventry and Warwickshire NHS Trust, CV2 2DX, Coventry, UK;

[3]Birmingham Heartlands and Solihull Hospitals, Heart of England NHS Foundation NHS Trust, B9 5SS, Birmingham, UK;

[4]Translational Research Institute, Hamad Medical Corporation, 3050, Doha, Qatar;

[5]Arden Tissue Bank, Pathology Department, University Hospitals Coventry and Warwickshire NHS Trust, CV2 2DX, Coventry, UK;

[6]Jining Medical University, 273100, Jining, PRC

[7]Aston Medical Research Institute, Aston Medical School, Aston University, B4 7ET, Birmingham, UK.

Abbreviated Title: Acetate promotes adipogenesis in brown adipocytes.

Key terms: Acetate, Adipogenesis, Mitochondrial Biogenesis, GPR43

Word count: 5347

Number of figures and tables: 8

Supplementary figures: 4

Corresponding authors:

Prof. Harpal S Randeva, MBChB, FRCP, Ph.D,

Warwick Medical School,

University of Warwick,

CV4 7AL, Coventry, United Kingdom

Phone: +44(0)2476-968862

Email: harpal.randeva@warwick.ac.uk

Dr. Jing Chen, Ph.D,

Warwick Medical School,

University of Warwick,

CV4 7AL, Coventry, United Kingdom

Phone: +44(0)2476-968693

Email: jing.chen@warwick.ac.uk

Disclosure Statement: The authors have nothing to disclose.

Abstract

Short-chain fatty acids play crucial roles in a range of physiological functions. However, the effects of short-chain fatty acids on brown adipose tissue have not been fully investigated. We examined the role of acetate, a short-chain fatty acid formed by fermentation in the gut, in the regulation of brown adipocyte metabolism. Our results show that acetate up-regulates AP2, PGC-1α and UCP1 expression and affects the morphological changes of brown adipocytes during adipogenesis. Moreover, an increase in mitochondrial biogenesis was observed after acetate treatment. Acetate also elicited the activation of ERK and CREB, and these responses were sensitive to G(i/o)-type G protein inactivator, Gβγ-subunit inhibitor, PLC inhibitor, PKC inhibitor and MEK inhibitor, indicating a role for the G(i/o)βγ/PLC/PKC/MEK signalling pathway in these responses. These effects of acetate were mimicked by treatment with 4-CMTB, a synthetic GPR43 agonist, and were impaired in GPR43 knock-down cells. Taken together, our results indicate that acetate may have important physiological roles in brown adipocytes through activation of GPR43.

Introduction

Short-chain fatty acids are a sub-group of fatty acids including formic acid, acetic acid, propionic acid, isobutyric acid, butyric acid, isovaleric acid and valeric acid. Acetate, propionate and butyrate are the three major short-chain fatty acids, which are mainly formed in the gastrointestinal tract via colonic bacteria fermentation of carbohydrates, especially resistant starches and dietary fibre (1). Following production in the gastrointestinal tract, short-chain fatty acids, especially acetate, may enter the circulation, be metabolized by peripheral tissues and directly affect energy homeostasis and metabolism. Given that it is the most abundant short-chain fatty acid produced in the colon, and that it partially avoids hepatic clearance, acetate can reach 150 μM concentrations in the peripheral circulation (2-7). Previous reports in humans show that, depending on the time of the day, the fasting/eating pattern and the glucose tolerance status of the individual, the circulating concentration of acetate could reach 100-150 μM with higher levels in arterial compared to venous blood (2-7). Circulating propionate and butyrate are detected in significantly lower levels (6), indicating that acetate mediates most of the short-chain fatty acids induced effects in peripheral tissues. Growing evidence indicates that short-chain fatty acids play important roles in a range of physiological functions, including neutrophil-driven inflammation (8), GLP-1 and PYY secretion (9,10), lipolysis and adipogenesis of white adipose tissue (11,12), and *de novo* synthesis of lipids and glucose (13).

Brown adipose tissue, also referred to as BAT or brown fat, is another type of adipose tissue primarily found in rodents and human infants. For a long time, BAT was perceived to quickly diminish after birth in humans; however, recent molecular and histological evidence have established that BAT remains present in adult humans (14). Subsequently, BAT has attracted attention as a novel target for the treatment of obesity and other obesity-related metabolic diseases due to its ability to generate heat by burning calories. Adipogenesis constitutes the process of cell differentiation by which pre-adipocytes become adipocytes. To date, it has been reported that adipogenesis of BAT is highly controlled by several

transcription factors, such as PPARγ and C/EBPs. A set of co-activators also regulates this process through their interaction with transcription factors [*e.g.* PPARγ coactivator-1α (PGC-1α) interacts with the transcription receptor PPAR-γ and regulates the genes involved in adipogenesis of BAT]. Of note, PGC-1α is highly expressed in brown, but not in white adipocytes. Furthermore, cold exposure or changes in nutritional status can dramatically up-regulate PGC-1α expression in BAT and skeletal muscle. Moreover, ectopically expressing PGC-1α in white adipocytes also induces 'browning' of their phenotype, indicating that PGC-1α plays an important role in the control of brown adipocyte differentiation. Finally, PGC-1α was also found to induce mitochondrial biogenesis, likely through the co-activation of a non-nuclear hormone receptor transcription factor, nuclear respiratory factor-1 (NRF-1), in brown adipocytes (15). Interestingly, data from clinical trials have suggested that increased PPARγ activity by thiazolidinediones (TZDs) also stimulates substantial adipogenesis in addition to reducing hyperglycemia in type 2 diabetic patients (16,17). Therefore, increasing the amount and/or activity of PGC-1α is also considered a potential useful pharmacologic strategy for the treatment of obesity-related diseases.

G protein-coupled receptors (GPCRs) constitute a family of seven transmembrane receptors. GPCRs play an important role in various signalling pathways by transducing a spectrum of extracellular signals to heterotrimeric G proteins, which further transduce these to appropriate downstream effectors in a signalling cascade (18). G-protein-coupled receptor 43 (GPR43), also called free fatty acid receptor 2 (FFA2/FFAR2), was deorphanized as a GPCR recognizing short-chain fatty acids, i.e. acetate and propionate, simultaneously by three independent groups (19-21). GPR43 reportedly couples to either Gi/o or Gq signalling pathways (19) and is highly expressed in immune cells and regulates inflammatory responses (8,22,23). GPR43 has also been reported to be expressed in adipose tissue. Previous data have demonstrated that activation of GPR43 promotes white adipocyte differentiation, leptin secretion in L-cells and inhibition of lipolysis in white adipose tissue (11), suggesting that short-chain fatty acids may

exert most, if not all, of their metabolic effects via GPR43 in white adipose tissue. However, there is little research on the role of short-chain fatty acids and GPR43 in BAT.

With the aforementioned in mind, we examined the effects of acetate in the regulation of brown adipocyte adipogenesis.

Materials and Methods

Reagents and Antibodies

Insulin, dexamethasone (Dex), isobutylmethylxanthine (IBMX), triiodothyronine (T3), and isopropanol were obtained from Sigma-Aldrich (Gillingham, UK). 4-chloro-α-(1-methylethyl)-N-2-thiazolylbenzeneacetamide (4-CMBT), U0126, U73122, pertussis toxin (PTX), and gallein were purchased from Tocris bioscience (Bristol, UK). The antibodies used in this study are listed in Table.1.

Animals

Male C57BL/6J (4 weeks old) mice were purchased from Dakewe Biotech Co., Ltd (Beijing, China). After a 2-week quarantine, the C57BL/6J mice were fed normal diet/chow until 12 weeks of age before tissue harvest. For acetate administration, 6-week-old mice were treated with sodium acetate (150 mM) in drinking water for 6 weeks (n = 5 for control, n = 5 for acetate administration). All of the mice were housed in the animal facility with a 12-h light/dark cycle and constant temperature (22–24°C). The mice had free access to water and diet. All procedures were approved by Jining Medical University and met the standards of the Guide for the Care and Use of Laboratory Animals issued by the Ministry of Science and Technology of the People's Republic of China in 2006.

Cell Isolation and Culture

The immortalized brown adipocyte cells line (IM-BAT) was provided by Dr Mark Christian (University of Warwick). Briefly, as previously described (24), primary cultures of brown adipocytes were generated by first digesting the interscapular BAT from male C57BL/6 mice with Tissue Dissociation Buffer

(DMEM/F12 medium containing collagenase (10 mg/ml) and DNase (10 mg/ml)) and pelleting the stromal vascular fraction (SVF) by centrifugation at 170×g for 10 min. Preadipocytes were purified by collecting the cells that passed through 100 μM of mesh. Next, brown preadipocytes were selected by collecting the cells that passed through 70 μM of mesh and were cultured in DMEM/F12 medium containing 10% FBS and 1% antibiotic-antimycotic for 2 days before being immortalized by retroviral-mediated expression of temperature-sensitive SV40 large T antigen H-2kb-tsA58. Cells were continually cultured at 33˚C and selected with G418 (100 mg/ml) for 2 weeks and maintained in 50 μg/ml of G418. Cells were differentiated by treating cells with differentiation medium I (DMEM/F12 containing 3-isobutyl-1-methylxanthine (IBMX, 500 μM), dexamethasone (250 nM), insulin (170 nM), 3,3',5-triiodo-l-thyronine (T3, 1 nM) and 10% FBS) for 48 h, followed by feeding cells with differentiation medium II (DMEM/F12 containing insulin (170 nM), T3 (1 nM) and 10% fetal bovine serum) every 2 days. To test the effects of acetate or 4-CMTB, replicate wells were incubated with acetate (10 mM) or 4-CMTB (10 μM), in combination with differentiation medium II in parallel. Differentiation was completed till clear lipid droplets could be seen under microscopy. All experiments were performed between passages 12 and 22.

Oil Red O staining

Lipid accumulation of differentiated adipocytes was visualized and determined by quantitative Oil red O staining kit (Millipore ECM950, Billerica, USA). Briefly, culture plates were washed in PBS, and fixed in 3.7% formaldehyde for 15 min, followed by staining with Oil Red O solution for 15 min. After staining, plates were washed twice with water and photographed. Oil red O was eluted using Dye Extraction Solution (100% isopropanol), and absorbance at 490 nm was measured.

Real time analysis using the xCELLigence system

The xCELLigence RTCA DP system (ACEA, San Diego, USA) was initialized as per manufacturer's instructions prior to measurements. E-plate was filled with basal medium (100 μl/well) and equilibrated at room temperature for 30 min. The E-plate was placed back into the DP station cradle (housed in a

humidified incubator at 37 ˚C with a 5% CO_2 atmosphere) to establish the background reading. IM-BAT cells were plated into E-plate at 5×10^4 cells per well in 100 μl aliquots. The E-plate was equilibrated at room temperature for 30 min before moved back into the DP station cradle. Cells were treated with differential medium I as described above for 2 days, followed by incubation with differential medium II only or with acetate/4-CMTB until day 7 post-induction. The xCELLigence system monitors the electrical impedance of gold sensing electrode underneath the cultured cell layer and calculates arbitrary cell index (*CI*) units as follows: CI = (Zi-Z0) / 15, in which Zi represents the electrical impedance at given time points and Z0 constitutes the background electrical impedance. The differentiation of IM-BAT cells in E-plate were also confirmed by optical microscope observation.

Cell viability assay

The MTS assay was performed in a time-course manner to determine the number of viable cells in culture. IM-BAT cells were seeded in 96-well plates at a density of 5×10^4 cells/well and treated with differentiation medium I for 2 days after cells reached confluence. Then cells were incubated with differentiation medium II for another 5 days. The CellTiter 96®AQ_{ueous} One Solution Reagent (Promega, Fitchburg, USA) was added into each well and the absorbance was measured at 490 nm in a plate reader to determine the formazan concentration, which is proportional to the number of living cells in culture.

Quantitative real-time PCR

Total RNA was isolated using GenElute™ Mammalian Total RNA Miniprep Kit (Sigma-Aldrich, Gillingham, UK). To degrade genomic DNA, a DNase digestion was performed with Precision DNase kits (Primerdesign, Southampton, UK). Up to 2 μg of total RNA was reverse transcribed in 20 μL using the Precision nanoScript Reverse Transcription kits (Primerdesign, Southampton, UK). A portion of reverse transcription reaction product was amplified to a total volume of 20 μL containing 250 nM of each primer and 1× SYBR green PCR master mix (Applied Biosystems, Waltham, USA). Analysis of gene expression was carried out in ABI 7500 Fast Real-Time PCR System with initial denaturation at 95 °C for 20 s, followed by 40 PCR cycles, each cycle consisting of 95 °C for 3 s and 60 °C for 30 s, and

SYBR green fluorescence emissions were monitored after each cycle. mRNA expression levels were calculated relative to the expression of the housekeeping gene 60S ribosomal protein L19 (*RPL*19). Amplification of specific transcripts was confirmed by the melting-curve profiles (cooling the sample to 60 °C and heating slowly to 95 °C with measurement of fluorescence) at the end of each PCR.

Measurement of Mitochondrial DNA by Quantitative Real-time PCR

DNA was isolated from differentiated IM-BAT cells using QIAamp DNA Mini Kit (QIAgen, Hilden, Germany). The mitochondrial DNA level was measured with primers targeted for mouse mitochondrial D-Loop with 1× SYBR green PCR master mix (Applied Biosystems, Waltham, USA) in ABI 7500 Fast Real-Time PCR System as described above. The mitochondrial DNA levels were normalized against the nuclear DNA level measured with 18S primers using the comparative C_T method.

Measurement of Mitochondrial Mass by Flow Cytometry

Preadipocytes were grown to confluence and differentiated as described above for 7 days. The fully differentiated cells were incubated with 50 nM CytoPainter MitoNIR Indicator Reagent (abcam, Cambridge, UK) in DMEM/F12 medium for 30 min at 37 °C. Cells were then washed with PBS, trypsinised, centrifuged, and resuspended in DMEM/F12 medium. Cells were analysed by Beckman Coulter FC500 flow cytometers, and CytoPainter MitoNIR Indicator Reagent fluorescent intensity was measured in FL4 channel.

XF24 Bioenergetic Assay

The oxygen consumption rate (OCR) measurements were performed by the Seahorse XF24 analyzer (Seahorse Bioscience, Copenhagen, Denmark). After the baseline measurement, testing agent (a-oligomycin; b-FCCP; c-antimycin A & rotenone) prepared in assay medium was then injected into each well to reach the desired final concentration. The XF24 protocol consists of three measurements of OCR (1 measurement/ 2 min); injection of oligomycin, and three measurements of OCR (1 measurement/ 2 min); injection of FCCP, and five measurements of OCR (1 measurement/ 2 min); injection of antimycin

& rotenone, and three measurements of OCR (1 measurement/ 2 min). The protein content of IM-BAT was measured after the XF24 bioenergetic assay and used for normalization.

Western blot

For western blot analyses, cells were lysed in RIPA buffer in the presence of phosphatase and protease inhibitors. The lysates were centrifuged at 14,000 g for 10 min at 4 ˚C and the supernatant fractions were used for collection. Samples containing equal amounts of protein were resolved in SDS-PAGE and then transferred onto Amersham Hybond ECL membrane. The membranes were blocked in 5% skimmed milk for 1h at room temperature and probed with specific antibodies overnight at 4 ˚C. Horseradish peroxidase conjugated anti-rabbit or anti-mouse secondary antibodies (Sigma-Aldrich, Gillingham, UK) and ECL Western Blotting Substrate (Pierce, Waltham, USA) were used to visualize specific protein bands. ECL results were captured by G:BOX Chemi XX6 system and quantitated using GeneTools software.

Immunohistochemistry staining

Brown adipose tissue of adult male c57bl/6 mice was immediately removed after sacrifice, and fixed in 10% buffered formalin. After fixation tissues were dehydrated in graded alcohol and embedded in paraffin. Embedding of tissues was performed by a paraffin dispenser DP 500 (Bio-Optica, Milano, Italy). The two-stage immunoperoxidase method was applied with ImmunoCruz rabbit ABC staining system (Santa Cruz, Dallas, USA). Briefly, paraffin-embedded adipose tissue was cut into 3 µm thick tissue sections using a rotary microtome Lecia RM2235 (Leica Microsystems, Milton Keynes, UK), which were deparaffinised and re-hydrated. Heat-induced antigen retrieval was performed prior to staining. In order to inhibit endogenous peroxidase activity slides were incubated in 3% solution of hydrogen peroxide for 10 minutes. Subsequently, non-specific antibody binding sites were blocked by incubation in goat serum for 30 minutes. The sections were incubated with the primary antibody (Polyclonal anti-GPR43 (Santa Cruz, Dallas, USA) antibody, dilution (1:125)) overnight at 4˚C. Subsequently the sections were washed in PBS (5 x 3 min) and incubated with the secondary (peroxidase-conjugated) antibody for 60 min at room temperature. Peroxidase activity was detected using the DAB technique (Liquid DAB substrate-

chromogen system). Nuclei were counterstained with haematoxylin. Control sections were similarly treated with omission of the primary antibody.

Phospho-kinase Proteome Profiling Assay

IM-BAT cells were differentiated and treated with or without acetate (10 mM) for 10 min. Cell lysates were prepared as described above and applied to phospho-kinase array following the manufacturer's instructions (R&D Systems). The phospho-kinase array results were developed by G:BOX Chemi XX6 system (Sysgene) and quantitated using GeneTools software (Sysgene).

Knockdown of GPR43 in IM-BAT cells

For establishing a knockdown of GPR43, immortalized IM-BAT cells were transfected with pLKO.1-puro non-mammalian control, or pLKO.1 encoding shRNAs targeting GPR43 (clone IDs TRCN0000027541, TRCN0000027552, TRCN0000027562, TRCN0000027581) using TransIT-2020 reagent from Mirus Bio LLC (Madison, USA) following the manufacturer's instructions. 24h post transfection, transfected cells were selected by adding 6 μg/ml puromycin. Each shRNA-encoding vector was transfected in triplicate wells. Cells were differentiated for 7 days. After harvesting the cells in Qiazol, the mRNA was isolated for real-time PCR analysis. Relative changes of GPR43 expression compared to the pLKO.1 control were normalized to the expression of RPL19 and quantified using the $2^{-\Delta\Delta Ct}$ method.

Statistical analysis

Results are presented as the mean ± S.E.M of at least triplicate samples in each experimental group; experiments were replicated to ensure consistency. Statistical significance of difference was determined using student's t test when comparing 2 groups or one-way ANOVA followed by post-hoc Tukey's multiple comparison test when comparing more than 3 groups. Values were considered to be statistically significant if their P value was less than 0.05. Statistical analyses were performed in GraphPad Prism 6 (GraphPad Software Inc., San Diego, CA).

Results

GPR43 is expressed in brown adipose tissue and immortalized brown adipocytes

GPR41 and GPR43 have been de-orphaned as short-chain fatty acids receptors. To test the hypothesis that GPR41 and/or GPR43 mediate the regulatory effects of acetate, real-time PCR analysis was performed on BAT to measure mRNA expression levels of GPR41 and GPR43. Our results demonstrated that GPR43 mRNA expression reached a clearly detectable level in BAT. The significant decrease of amplification products in minus-reverse transcriptase (-RT) controls confirmed that the PCR amplification is mostly attributable to the presence of GPR43 cDNA (Fig.1A). To clarify that GPR43 was expressed in brown adipocytes instead of stromal vascular fraction, isolated brown adipocytes were also used to analyse the mRNA expression of GPR43. The mRNA transcription was quantified in immortalized brown adipocytes during the course of adipose differentiation until 9 days induction of differentiation (Fig.1B). Our western blot results also show that GPR43 expression was scarcely detected in pre-adipocytes (Day 0) but significantly increased after differentiation induction (Fig.1C). We were unable to detect any GPR41 expression which is in agreement with previous studies (25). Immunohistochemical staining was also used to demonstrate the existence of GPR43 in brown adipose tissue. As shown in Fig.1D, immunoperoxidase staining of formalin-fixed, paraffin-embedded mice brown adipose tissue using anti-GPR43 antibody shows membrane and cytoplasmic staining, while in the no primary antibody control, only negligible staining could be found.

Activation of GPR43 during differentiation of IM-BAT increases PGC-1α and UCP1 expression

In order to examine the effects of acetate on differentiating brown adipocytes, IM-BAT cells were treated with or without acetate (10 mM) throughout the course of the differentiation process from day 2 until day 7 post-induction, at which time the hypertrophic brown adipocytes filled with plenty of lipid droplets (Supplementary Fig.1). Lipid accumulation in differentiated brown adipocytes was measured using Oil red O staining kit. As shown in Fig.2A, acetate increased Oil red O staining of IM-BAT cells after differentiation relative to normally-differentiated control cells, indicating acetate as a positive modulator

of brown adipocyte development. Furthermore, the expression of several adipogenesis-related and thermogenesis-related genes was also examined. As shown in Fig.2B, acetate treatment during brown adipocyte differentiation (from day 2) significantly increased the mRNA expression levels of PPARγ, AP2, PGC-1α, and UCP1. In addition, we also treated IM-BAT cells with 4-CMTB during the differentiation, a selective agonist for GPR43 (26). As shown in Fig.2C, 4-CMTB treatment also increased the expression of AP2, PGC-1α and UCP1, whilst the PPARγ expression also showed an increasing trend. The mRNA expression of BMP7 and PRDM16 did not show any significant changes with either acetate or 4-CMTB treatments. Protein expression of PGC-1α and UCP1 was also tested after acetate treatment. Our results demonstrated that the protein levels of PGC-1α and UCP1 exhibited ~1.9 fold and ~2.3 fold increases, respectively, in acetate treated cells compared to normally-differentiated cells (Fig.2D). 4-CMTB treatment also showed an increase of PGC-1α and UCP1 protein expression (Fig.2E). Concentration-dependent effects of acetate treatment on PGC-1α and UCP1 during brown adipogenesis were also investigated in immortalized brown adipocytes. As shown in Supplementary Fig.2, compared to the effects of 10 mM acetate treatment, acetate at 1mM also induced a pronounced increase of PGC-1α and UCP1, while the lower concentration of acetate induced a relatively weaker response on PGC-1α and UCP1 expression (Supplementary Fig.2). Overall these findings suggest that activation of GPR43 during IM-BAT differentiation augments the expression of key adipogenesis markers, such as AP2, and brown adipocyte markers, i.e. PGC-1α and UCP1. Moreover, we also examined the effects of acetate on the expression of these two thermogenesis-related genes (PGC-1α and UCP1) in BAT *in vivo*. These results demonstrated a significant increase in PGC-1α ($p=0.016$), while the increase in UCP1 expression just failed significance ($p=0.076$; Fig.2F). Furthermore, acute acetate treatment (6h) on differentiated IM-BAT cells also significantly increased PGC-1α ($p=0.013$) and UCP1 transcription ($p=0.028$; Fig.2G).

Activation of GPR43 during differentiation of IM-BAT affects the morphological shift of brown adipocytes during adipogenesis

The xCELLigence system monitors the electrical impedance of gold sensing electrode underneath the cultured cell layer and calculates arbitrary cell index (*CI*) units, which are affected by the number, shape, adhesion, and/or mobility of the adherent cells. The *CI* value of IM-BAT cells significantly dropped after the incubation with differentiation medium I (Fig. 3A), as previously reported by Kramer AH et al. for differentiation of 3T3-L1 cells (27). Interestingly, the *CI* curves of IM-BAT cells rapidly increased followed by a slightly decrease after incubation with differentiation medium II. Furthermore, both acetate and 4-CMTB treatment during the incubation with differentiation medium II dramatically decreased the rise of *CI* compared to control. Cell death was ruled out as a cause for this decrease of *CI* values since cell viability was confirmed by MTS assay (Fig.3B), indicating that the cell shape or adhesion instead of the cell number contributes more to the difference of *CI* values.

Activation of GPR43 during differentiation of IM-BAT increased mitochondrial biogenesis in brown adipocytes

Mitochondrial biogenesis has been associated with brown adipocyte differentiation and thermogenesis. PGC-1α is a key co-activator to turn on this process in brown adipocytes. Thus, we examined the effects of acetate treatment on mitochondrial biogenesis in brown adipocytes. As shown in Fig.4A and B, the mitochondrial DNA to nuclear DNA ratio was increased after IM-BAT cells treated with acetate or 4-CMTB during the differentiation period from day 2 until day 7. In agreement with this result, the flow cytometry assay also documented increased mitochondrial mass in brown adipocytes after acetate treatment during differentiation (Fig.4C). Furthermore, the basal oxygen consumption rate (OCR) and spare respiratory capacity (stimulated by FCCP) in acetate treated cells were increased by 17%, and 24%, respectively (Fig.4D). More pronounced increases of the basal OCR and reserve respiratory capacity were also observed after 4-CMTB treatment during the differentiation of IM-BAT cells (Fig.4E). The IM-BAT cells differentiated with acetate treatment also show increased OCR upon β-adrenergic receptor agonist CL316,243 treatment (Supplementary Fig.3). These observed mitochondrial responses might also reflect

increased mitochondria mass. These data consistently support the role of acetate activity in promoting mitochondrial biogenesis.

Activation of GPR43 activate ERK1/2 and CREB in differentiated brown adipocytes

To determine the signalling pathways activated following acetate exposure in brown adipocytes, Proteome Profiler phospho-kinase array spotted with antibodies against 43 different kinases and 2 related total proteins (R&D Systems) was utilized. As shown in Fig.5A, the phosphorylation of ERK1/2 and CREB (S133) increased by ~2.0 fold and ~2.6 fold vs. untreated cells, respectively, after 10 mM acetate treatment for 10 min in differentiated brown adipocytes, suggesting increased activation of these two kinases by acetate. To further determine the time course of ERK1/2 phosphorylation and CREB activation in IM-BAT cells after acetate stimulation, cells were treated with 10 mM acetate from 5 to 60 min. This experiment revealed that acetate increased p-ERK1/2 within 5 min and sustained a high level for 30 min (Fig.5B). Furthermore, we also observed that CREB phosphorylation increased starting from 5 min and stayed at peaking level at 10 min (Fig.5B). Similarly, 4-CMTB treatment also elicits the phosphorylation of ERK1/2 and CREB in brown adipocytes (Fig.5C). It is well-established that activation of CREB enhances PGC-1α expression in a CREB-dependent manner (28). Therefore, these data consistently suggest that ERK1/2 and CREB were activated by acetate and that their activation may contribute to the increase in PGC-1α activity.

GPR43 knock-down impaired the effects of acetate or 4-CMTB on brown adipocytes

To further assess the role of GPR43 in acetate-induced effects on brown adipocytes, we transfected IM-BAT cells with GPR43 shRNA and selected with puromycin. Using shRNA for GPR43, we successfully decreased gene expression to less than 30% of its baseline value in differentiated adipocytes (Fig.6A). We examined the effects of acetate treatment on mitochondrial biogenesis in IM-BAT with impaired GPR43 expression (sh-GPR43-1) adipocytes. While the stimulatory effect of acetate on UCP1 mRNA was apparent in control cells, this effect was impaired in cells transfected with shRNA for GPR43 (Fig.6B). The stimulatory effect of acetate treatment on mitochondrial content was also significantly reduced in sh-

GPR43-1 adipocytes (Fig. 6C). Similarly, although acetate increased ERK1/2 and CREB phosphorylation, there was no such stimulation in cells in which the GPR43 gene had been knocked-down (Fig.6D). These results consistently support the hypothesis that GPR43, and not GPR41, is mainly involved in acetate-mediated effects in IM-BAT cells.

ERK1/2 activation is required for SCFA-induced CREB phosphorylation

Several studies have demonstrated that ERK1/2 is located upstream of CREB (29,30). Having defined both ERK1/2 and CREB phosphorylation as a consequence of acetate treatment, we sought next to elucidate whether ERK1/2 activation is required for SCFA evoked CREB phosphorylation. For this purpose, the MEK1/2 inhibitor U0126 was used to block the phosphorylation of ERK1/2. As shown in Fig.7A, although treatment of brown adipocytes with acetate caused the expected increase in ERK and CREB phosphorylation, acetate was unable to induce CREB phosphorylation in cells pre-treated with U0126, while ERK phosphorylation was almost completely abolished. These results indicate that ERK1/2 is a major mediator of SCFA-induced CREB phosphorylation.

Phosphorylation of ERK and CREB is dependent of the $G_{(i/o)}\beta\gamma$/PLC/PKC/MEK signalling pathway

Previous research has demonstrated that GPR43 couples to both G_q and G_i proteins, which interact with several downstream molecules (including adenylate cyclase, and phospholipase C) (31). As shown in Fig.7B, pre-treatment with pertussis toxin (PTX), a $G_{i/o}$-type G protein inactivator, significantly attenuates both ERK1/2 and CREB phosphorylation induced by acetate. It is reported that $G_{i/o}$ mediates the PLC-PKC-ERK1/2 pathway via its βγ subunits (32). Therefore, we also examined the effects of pre-treatment with Gallein ($G_{(i/o)}\beta\gamma$ inhibitor), and U73122 (PLC inhibitor) on acetate-induced ERK and CREB activation. Our results show that acetate-induced CREB activation was effectively blocked by these inhibitors (Fig.7C & D). Taken together, these results suggest that the G(i/o)βγ/PLC/PKC pathway plays a crucial role in acetate induced ERK and CREB activation.

Discussion

Short-chain fatty acids are considered important energy sources, especially for colonocytes. Recent evidence further revealed that short-chain fatty acids also mediate a spectrum of physiological functions as signalling molecules (33). Several studies have established strong links between short-chain fatty acids and energy metabolism. Accordingly, Ikuo Kimura et al. reported that short-chain fatty acids increase energy expenditure in both the liver and muscle in mice (34). Another *in vivo* study in mice also found that dietary supplementation of propionic acid and butyric acid protects against high fat diet-induced obesity via inhibiting food intake, improving insulin sensitivity and increasing energy expenditure (35). Additional studies also show that acetate reduces appetite via regulating neuropeptides which favour appetite suppression (7). These findings suggest that short-chain fatty acids, through activation of their receptors, regulate important signalling pathways involved in energy expenditure and homoeostasis. The present study demonstrates that acetate stimulates mitochondrial biogenesis with up-regulation of PPARγ, PGC-1α and UCP1 expression in brown adipocytes, suggesting that short-chain fatty acids could function as regulators of adipogenesis in brown adipocytes development and differentiation. Our results provide novel insight to understand the regulatory effects of short-chain fatty acids in energy metabolism.

PPARγ has been shown to be critical for adipogenesis in various adipocyte models, however, it does not induce adipogenesis alone (36). PGC-1α, a transcription co-activator, is a key molecule that stimulates brown adipocytes differentiation and interacts with PPARγ and direct gene transcription involved in both adipogenesis and mitochondrial biogenesis (37). Increased PGC-1α enhances the transcription of NRF-1 and NRF-2, leading to increased expression of mtTFA (15), as well as other nuclear-encoded mitochondria subunits of the electron transport chain complex (*e.g.* β-ATP synthase, cytochrome c, and cytochrome c oxidase IV) (38). mtTFA translocates to the mitochondrion and stimulates mitochondrial DNA replication and gene expression (39). PGC-1α also interacts with PPARγ or other nuclear hormone receptors in BAT to up-regulate the expression of brown fat-specific UCP1 (40,41). Our results show that

increased PGC-1α expression, as well as increased mitochondrial mass and UCP1 expression were observed after acetate treatment in brown adipocytes, suggesting the importance of PGC-1α in brown adipocyte differentiation. However, our findings are speculative that dietary supplementation of acetate could potentially promote BAT by increasing the amount and/or activity of PGC-1α, thus offering an additional target for the treatment of obesity and related metabolic diseases. Further studies are needed to determine whether acetate actions on UCP1 or mitochondrial biogenesis are PGC-1α mediated. Moreover, additional studies are also required to delineate the potential effects of other short chain fatty acids, such as butyrate and propionate, on brown adipose tissue.

Furthermore, Kramer AH et al. have shown that the morphological changes during 3T3-L1 differentiation could be monitored by the xCELLigence system (27). Treatment with a similar differentiation cocktail (containing insulin, IBMX, Dexamethasone, and Rosiglitazone) leads to a rapid drop of the *CI* curve of 3T3-L1 cells (27), which seems to be necessary for successful differentiation of 3T3-L1 adipocytes. In this study, a similar *CI* curve was also observed after the treatment of IM-BAT cells with differentiation medium I containing insulin, IBMX, Dexamethasone, and T3. Kramer AH *et al.* have further established that among the components of the full differentiation cocktail, treatment with IBMX only resulted in a *CI* profile similar to the one after treatment with the full differentiation cocktail, indicating that IBMX mainly mediate the *CI* change of 3T3-L1 during the differentiation (27). Our findings are also in accord with this finding, since an increased *CI* value was observed after the incubation with differentiation medium II, which does not contain IBMX. In addition, our results also demonstrated that acetate treatment could maintain the *CI* value at a lower level compared to normal differentiation control cells. Based on the previous data from 3T3-L1 cells, documenting that the most efficient differentiation caused by the full differentiation cocktail results in the most decreased *CI* value, our results indicate that the decreased *CI* value might reflect promotive effects of acetate on the differentiation of IM-BAT cells.

These results suggest that IM-BAT cells undergo morphological shifts during the differentiation and activation of GPR43 could affect this process.

Moreover, our results further identified ERK/CREB signalling pathways in the underlying mechanism by which GPR43 receptors regulate this response. GPR43 shares 38% identity with GPR41 in amino acid sequence and recognizes short-chain fatty acids (42). Based on our experiments, we could not observe GPR41 expression at detectable levels in brown adipocytes. This finding is consistent with previous data reporting that nearly all identified physiological functions of short-chain fatty acids in white adipocytes were mediated by GPR43. Notably, Choi SH *et al.* reported that co-culture of adipocytes with myoblasts promotes C/EBPβ and PPARγ gene expression in differentiated myoblasts and GPR43 expression in adipocytes, also suggesting that GPR43 might be involved in adipogenesis via mediating PPARγ activity (43).

Previous data have also reported that G(i/o)βγ mediates the PLC-PKC-ERK signalling pathway. Our findings indicate that this G(i/o)βγ mediated PLC-PKC-ERK signalling pathway is necessary for acetate induced CREB phosphorylation. It has been well-studied that phosphorylation of CREB leads to increased PGC-1α expression in a CREB-dependent manner (28). Therefore, our data consistently suggest that ERK1/2 and CREB activation may be the underlying mechanism of the increase in PGC-1α.

It is noteworthy that both GPR43-dependent and -independent mechanisms have been shown to mediate pro-adipogenic effects of short-chain fatty acids on different adipose tissues. For example, short-chain fatty acids have been reported to promote adipogenesis via inhibiting histone deacetylases (44), whilst the conversion of acetate to acetyl-CoA also plays a role in lipid synthesis and energy generation. Therefore, GPR43-independent mechanisms may also be mediating short-chain fatty acid-induced effects in brown adipose tissue.

Finally, we employed a purely classical infrascapular brown adipose tissue precursors system for our experiments. A limitation in the present study was the lack of access to a My5- "beige" precursor line which would have provided a more translational impact to our observations. Indeed, Jun Wu *et al*. suggested that there are two distinct types of brown fat: classical brown fat derived from a myf-5 cellular lineage and UCP1-positive cells that emerge in white fat from a non-myf-5 lineage (45). These authors cloned “beige” cells from murine white fat depots which respond to cyclic AMP stimulation with high UCP1 expression and respiration rates. In the context of our study in order to establish that the observed effects are not cell line dependent, we also performed experiments using an additional brown adipocyte model (T37i) in which we also documented increased PGC1α and UCP1 expression upon acetate stimulation (Supplementary Fig.4).

In conclusion, the present study suggests that short-chain fatty acids play an important role in BAT differentiation. Further studies are required to clarify the mechanisms of action of short-chain fatty acids in adipogenesis of brown adipocytes.

Acknowledgments

H S R acknowledges funding support from the General Charities of the City of Coventry and is grateful to Dr Mark Christian, University of Warwick, for providing the IM-BAT cell line; and to Prof. Bo Bai, Jining University, for providing assistance for the animal experiments.

References

1. Wong JM, de Souza R, Kendall CW, Emam A, Jenkins DJ. Colonic health: fermentation and short chain fatty acids. Journal of clinical gastroenterology 2006; 40:235-243
2. Tollinger CD, Vreman HJ, Weiner MW. Measurement of acetate in human blood by gas chromatography: effects of sample preparation, feeding, and various diseases. Clinical chemistry 1979; 25:1787-1790
3. Pomare EW, Branch WJ, Cummings JH. Carbohydrate fermentation in the human colon and its relation to acetate concentrations in venous blood. J Clin Invest 1985; 75:1448-1454
4. Scheppach W, Pomare EW, Elia M, Cummings JH. The contribution of the large intestine to blood acetate in man. Clin Sci (Lond) 1991; 80:177-182
5. Peters SG, Pomare EW, Fisher CA. Portal and peripheral blood short chain fatty acid concentrations after caecal lactulose instillation at surgery. Gut 1992; 33:1249-1252
6. Wolever TM, Josse RG, Leiter LA, Chiasson JL. Time of day and glucose tolerance status affect serum short-chain fatty acid concentrations in humans. Metabolism 1997; 46:805-811
7. Frost G, Sleeth ML, Sahuri-Arisoylu M, Lizarbe B, Cerdan S, Brody L, Anastasovska J, Ghourab S, Hankir M, Zhang S, Carling D, Swann JR, Gibson G, Viardot A, Morrison D, Louise Thomas E, Bell JD. The short-chain fatty acid acetate reduces appetite via a central homeostatic mechanism. Nat Commun 2014; 5:3611
8. Sina C, Gavrilova O, Forster M, Till A, Derer S, Hildebrand F, Raabe B, Chalaris A, Scheller J, Rehmann A, Franke A, Ott S, Hasler R, Nikolaus S, Folsch UR, Rose-John S, Jiang HP, Li J, Schreiber S, Rosenstiel P. G protein-coupled receptor 43 is essential for neutrophil recruitment during intestinal inflammation. Journal of immunology 2009; 183:7514-7522
9. Tolhurst G, Heffron H, Lam YS, Parker HE, Habib AM, Diakogiannaki E, Cameron J, Grosse J, Reimann F, Gribble FM. Short-chain fatty acids stimulate glucagon-like peptide-1 secretion via the G-protein-coupled receptor FFAR2. Diabetes 2012; 61:364-371
10. Psichas A, Sleeth ML, Murphy KG, Brooks L, Bewick GA, Hanyaloglu AC, Ghatei MA, Bloom SR, Frost G. The short chain fatty acid propionate stimulates GLP-1 and PYY secretion via free fatty acid receptor 2 in rodents. International journal of obesity 2014;
11. Ge H, Li X, Weiszmann J, Wang P, Baribault H, Chen JL, Tian H, Li Y. Activation of G protein-coupled receptor 43 in adipocytes leads to inhibition of lipolysis and suppression of plasma free fatty acids. Endocrinology 2008; 149:4519-4526
12. Hong Y-H, Nishimura Y, Hishikawa D, Tsuzuki H, Miyahara H, Gotoh C, Choi K-C, Feng DD, Chen C, Lee H-G, Katoh K, Roh S-G, Sasaki S. Acetate and Propionate Short Chain Fatty Acids Stimulate Adipogenesis via GPCR43. Endocrinology 2005; 146:5092-5099
13. den Besten G, Lange K, Havinga R, van Dijk TH, Gerding A, van Eunen K, Muller M, Groen AK, Hooiveld GJ, Bakker BM, Reijngoud DJ. Gut-derived short-chain fatty acids are vividly assimilated into host carbohydrates and lipids. American journal of physiology Gastrointestinal and liver physiology 2013; 305:G900-910
14. Cypess AM, Lehman S, Williams G, Tal I, Rodman D, Goldfine AB, Kuo FC, Palmer EL, Tseng YH, Doria A, Kolodny GM, Kahn CR. Identification and importance of brown adipose tissue in adult humans. The New England journal of medicine 2009; 360:1509-1517
15. Wu Z, Puigserver P, Andersson U, Zhang C, Adelmant G, Mootha V, Troy A, Cinti S, Lowell B, Scarpulla RC. Mechanisms controlling mitochondrial biogenesis and respiration through the thermogenic coactivator PGC-1. Cell 1999; 98:115-124
16. Nathan DM, Buse JB, Davidson MB, Ferrannini E, Holman RR, Sherwin R, Zinman B. Medical management of hyperglycemia in type 2 diabetes: a consensus algorithm for the initiation and

adjustment of therapy: a consensus statement of the American Diabetes Association and the European Association for the Study of Diabetes. Diabetes Care 2009; 32:193-203

17. Belcher G, Matthews DR. Safety and tolerability of pioglitazone. Exp Clin Endocrinol Diabetes 2000; 108:267-273

18. Tuteja N. Signaling through G protein coupled receptors. Plant Signaling & Behavior 2014; 4:942-947

19. Brown AJ, Goldsworthy SM, Barnes AA, Eilert MM, Tcheang L, Daniels D, Muir AI, Wigglesworth MJ, Kinghorn I, Fraser NJ, Pike NB, Strum JC, Steplewski KM, Murdock PR, Holder JC, Marshall FH, Szekeres PG, Wilson S, Ignar DM, Foord SM, Wise A, Dowell SJ. The Orphan G protein-coupled receptors GPR41 and GPR43 are activated by propionate and other short chain carboxylic acids. The Journal of biological chemistry 2003; 278:11312-11319

20. Le Poul E, Loison C, Struyf S, Springael JY, Lannoy V, Decobecq ME, Brezillon S, Dupriez V, Vassart G, Van Damme J, Parmentier M, Detheux M. Functional characterization of human receptors for short chain fatty acids and their role in polymorphonuclear cell activation. The Journal of biological chemistry 2003; 278:25481-25489

21. Nilsson NE, Kotarsky K, Owman C, Olde B. Identification of a free fatty acid receptor, FFA2R, expressed on leukocytes and activated by short-chain fatty acids. Biochemical and biophysical research communications 2003; 303:1047-1052

22. Maslowski KM, Vieira AT, Ng A, Kranich J, Sierro F, Yu D, Schilter HC, Rolph MS, Mackay F, Artis D, Xavier RJ, Teixeira MM, Mackay CR. Regulation of inflammatory responses by gut microbiota and chemoattractant receptor GPR43. Nature 2009; 461:1282-1286

23. Vinolo MAR, Ferguson GJ, Kulkarni S, Damoulakis G, Anderson K, Bohlooly-Y M, Stephens L, Hawkins PT, Curi R. SCFAs Induce Mouse Neutrophil Chemotaxis through the GPR43 Receptor. PLoS ONE 2011; 6:e21205

24. Rosell M, Kaforou M, Frontini A, Okolo A, Chan YW, Nikolopoulou E, Millership S, Fenech ME, MacIntyre D, Turner JO, Moore JD, Blackburn E, Gullick WJ, Cinti S, Montana G, Parker MG, Christian M. Brown and white adipose tissues: intrinsic differences in gene expression and response to cold exposure in mice. American journal of physiology Endocrinology and metabolism 2014; 306:E945-964

25. Zaibi MS, Stocker CJ, O'Dowd J, Davies A, Bellahcene M, Cawthorne MA, Brown AJH, Smith DM, Arch JRS. Roles of GPR41 and GPR43 in leptin secretory responses of murine adipocytes to short chain fatty acids. FEBS Letters 2010; 584:2381-2386

26. Smith NJ, Ward RJ, Stoddart LA, Hudson BD, Kostenis E, Ulven T, Morris JC, Tränkle C, Tikhonova IG, Adams DR, Milligan G. Extracellular Loop 2 of the Free Fatty Acid Receptor 2 Mediates Allosterism of a Phenylacetamide Ago-Allosteric Modulator. Molecular Pharmacology 2011; 80:163-173

27. Kramer AH, Joos-Vandewalle J, Edkins AL, Frost CL, Prinsloo E. Real-time monitoring of 3T3-L1 preadipocyte differentiation using a commercially available electric cell-substrate impedance sensor system. Biochemical and Biophysical Research Communications 2014; 443:1245-1250

28. Wu H, Kanatous SB, Thurmond FA, Gallardo T, Isotani E, Bassel-Duby R, Williams RS. Regulation of mitochondrial biogenesis in skeletal muscle by CaMK. Science 2002; 296:349-352

29. Xing J, Ginty DD, Greenberg ME. Coupling of the RAS-MAPK Pathway to Gene Activation by RSK2, a Growth Factor-Regulated CREB Kinase. Science 1996; 273:959-963

30. Impey S, Obrietan K, Wong ST, Poser S, Yano S, Wayman G, Deloulme JC, Chan G, Storm DR. Cross Talk between ERK and PKA Is Required for Ca2+ Stimulation of CREB-Dependent Transcription and ERK Nuclear Translocation. Neuron 1998; 21:869-883

31. Brown AJ, Goldsworthy SM, Barnes AA, Eilert MM, Tcheang L, Daniels D, Muir AI, Wigglesworth MJ, Kinghorn I, Fraser NJ, Pike NB, Strum JC, Steplewski KM, Murdock PR, Holder JC, Marshall FH, Szekeres PG, Wilson S, Ignar DM, Foord SM, Wise A, Dowell SJ. The Orphan G Protein-coupled Receptors GPR41 and GPR43 Are Activated by Propionate and Other Short Chain Carboxylic Acids. Journal of Biological Chemistry 2003; 278:11312-11319

32. Zhou Q, Li G, Deng XY, He XB, Chen LJ, Wu C, Shi Y, Wu KP, Mei LJ, Lu JX, Zhou NM. Activated human hydroxy-carboxylic acid receptor-3 signals to MAP kinase cascades via the PLC-dependent PKC and MMP-mediated EGFR pathways. British Journal of Pharmacology 2012; 166:1756-1773

33. den Besten G, van Eunen K, Groen AK, Venema K, Reijngoud D-J, Bakker BM. The role of short-chain fatty acids in the interplay between diet, gut microbiota, and host energy metabolism. Journal of Lipid Research 2013; 54:2325-2340

34. Kimura I, Ozawa K, Inoue D, Imamura T, Kimura K, Maeda T, Terasawa K, Kashihara D, Hirano K, Tani T, Takahashi T, Miyauchi S, Shioi G, Inoue H, Tsujimoto G. The gut microbiota suppresses insulin-mediated fat accumulation via the short-chain fatty acid receptor GPR43. Nat Commun 2013; 4:1829

35. Gao Z, Yin J, Zhang J, Ward RE, Martin RJ, Lefevre M, Cefalu WT, Ye J. Butyrate Improves Insulin Sensitivity and Increases Energy Expenditure in Mice. Diabetes 2009; 58:1509-1517

36. Bastie C, Holst D, Gaillard D, Jehl-Pietri C, Grimaldi PA. Expression of Peroxisome Proliferator-activated Receptor PPARδ Promotes Induction of PPARγ and Adipocyte Differentiation in 3T3C2 Fibroblasts. Journal of Biological Chemistry 1999; 274:21920-21925

37. Puigserver P, Wu Z, Park CW, Graves R, Wright M, Spiegelman BM. A cold-inducible coactivator of nuclear receptors linked to adaptive thermogenesis. Cell 1998; 92:829-839

38. Scarpulla RC. Transcriptional activators and coactivators in the nuclear control of mitochondrial function in mammalian cells. Gene 2002; 286:81-89

39. Larsson NG, Wang J, Wilhelmsson H, Oldfors A, Rustin P, Lewandoski M, Barsh GS, Clayton DA. Mitochondrial transcription factor A is necessary for mtDNA maintenance and embryogenesis in mice. Nature genetics 1998; 18:231-236

40. Barbera MJ, Schluter A, Pedraza N, Iglesias R, Villarroya F, Giralt M. Peroxisome proliferator-activated receptor alpha activates transcription of the brown fat uncoupling protein-1 gene. A link between regulation of the thermogenic and lipid oxidation pathways in the brown fat cell. The Journal of biological chemistry 2001; 276:1486-1493

41. Cassard-Doulcier AM, Larose M, Matamala JC, Champigny O, Bouillaud F, Ricquier D. In vitro interactions between nuclear proteins and uncoupling protein gene promoter reveal several putative transactivating factors including Ets1, retinoid X receptor, thyroid hormone receptor, and a CACCC box-binding protein. The Journal of biological chemistry 1994; 269:24335-24342

42. Sawzdargo M, George SR, Nguyen T, Xu S, Kolakowski Jr LF, O'Dowd BF. A Cluster of Four Novel Human G Protein-Coupled Receptor Genes Occurring in Close Proximity to CD22 Gene on Chromosome 19q13.1. Biochemical and Biophysical Research Communications 1997; 239:543-547

43. Choi SH, Chung KY, Johnson BJ, Go GW, Kim KH, Choi CW, Smith SB. Co-culture of bovine muscle satellite cells with preadipocytes increases PPARγ and C/EBPβ gene expression in differentiated myoblasts and increases GPR43 gene expression in adipocytes. The Journal of nutritional biochemistry 2013; 24:539-543

44. Li G, Yao W, Jiang H. Short-chain fatty acids enhance adipocyte differentiation in the stromal vascular fraction of porcine adipose tissue. J Nutr 2014; 144:1887-1895

45. Wu J, Bostrom P, Sparks LM, Ye L, Choi JH, Giang AH, Khandekar M, Virtanen KA, Nuutila P, Schaart G, Huang K, Tu H, van Marken Lichtenbelt WD, Hoeks J, Enerback S, Schrauwen P, Spiegelman BM. Beige adipocytes are a distinct type of thermogenic fat cell in mouse and human. Cell 2012; 150:366-376

FIGURE LEGENDS

Fig.1 (A) GPR43 mRNA expression was identified by real-time PCR from cDNA pool of brown adipose tissue (BAT). The minus-reverse transcriptase (minus-RT) control was introduced to exclude potential genomic DNA contamination. (B) The mRNA transcription levels of GPR43 increase in the course of adipogenesis of IM-BAT adipocytes. (C) Western blot analysis showing GPR43 expression in undifferentiated and differentiated IM-BAT cells. (D) Immunohistochemistry analysis showing GPR43 expression in brown adipose tissue. Data are presented as mean ± S.E.M.. *P <0.05, **P<0.01 compared to Day 0 by one-way ANOVA followed by Post-Hoc tests.

Fig.2. (A) IM-BAT cells were differentiated with or without acetate (10 mM) for 7 days and stained by Oil Red O. The Oil Red O was extracted and the absorbance was measured in a plate reader at 490 nm. (B and C) Relative mRNA levels of brown adipocyte markers in IM-BAT cells treated with or without acetate (B) or 4-CMTB (C) during differentiation. (D and E) PGC-1α and UCP1 protein levels in IM-BAT cells treated with or without acetate (D) or 4-CMTB (E) during differentiation. (F) Effects of acetate administration on PGC-1α and UCP1 expression in interscapular brown adipose tissue of C57BL/6J male mice (n = 5 for control, n = 5 for acetate administration). (G) Effects of acute acetate treatment (6 h; 10 mM) on PGC-1α and UCP1 expression in differentiated IM-BAT cells. β-adrenergic receptor agonist CL-316,243 (CL) was used as positive control. Data are presented as mean ± S.E.M.. *P <0.05, **P<0.01, ***P<0.001 by student's t-test compared with no acetate treated controls.

Fig.3 (A) Effects of acetate on immortalized BAT (IM-BAT) cell growth *CI* curves during differentiation. IM-BAT cells were treated with differential medium I followed by Insulin + T3 (top); or Insulin + T3 + Acetate (middle); or Insulin + T3 + 4-CMTB (bottom) at the same time to compare the resulting *CI* growth curves. All curves were plotted as the average of quadruplicate treatments, with error bars shown as S.E.M. (n = 4). Compared to Insulin + T3, the Insulin + T3 + Acetate and the Insulin + T3 + 4-CMTB

arms of the experiment showed much lower *CI* values. (B) Cell viability of IM-BAT cells after differentiation was measured by the MTS assay. Values presented as mean ± S.E.M.. ns = non-significant to control group.

Fig.4 (A & B) Relative mitochondrial DNA levels in immortalized BAT (IM-BAT) cells treated with or without acetate (A) or 4-CMTB (B) during differentiation from day 2 until day 7 post-induction. (C) Mitochondrial mass of IM-BAT cells, treated with acetate during differentiation from day 2 until day 7 post-induction, was measured by flow cytometry and compared with untreated cells by fluorescence levels upon staining with CytoPainter MitoNIR Indicator Reagent. (D & E) The effect of acetate (D) or 4-CMTB (E) treatment on mitochondrial respiratory capacity of IM-BAT during differentiation measured by the XF24 analyzer. Group mean oxygen consumption rate (OCR) in pMol/min/μg protein of IM-BAT cells treated with or without acetate at 10 mM during differentiation from day 2 to day 7. Vertical lines indicate time of addition of mitochondrial inhibitors (a) oligomycin (1 μM), (b) FCCP (0.5 μM), or (c) antimycin A (1 μM) & rotenone (1 μM). Basal OCR, maximum OCR, spare capacity of cells treated as described above. Values presented as mean ± S.E.M.. * $P < 0.05$ by student's t-test.

Fig.5 (A) Immortalized BAT (IM-BAT) cells were differentiated for 5 days and either left untreated or treated with acetate for 10 minutes. Site-specific phosphorylation of 43 kinases were analysed by R&D Proteome Profiler Phospho-Kinase Array Kit. (B) Time-course of ERK and CREB activation following treatment with acetate in IM-BAT cells. Differentiated IM-BAT cells were either left untreated or treated with acetate for 5, 10, 15, 30 and 60 minutes. (C) Time-course of ERK and CREB activation following treatment with 4-CMTB in IM-BAT cells. Differentiated IM-BAT adipocytes were either left untreated or treated with 4-CMTB for 5, 10, 15, 30 and 60 minutes. Data are presented as mean ± S.E.M.. *$P < 0.05$, **$P<0.01$, ***$P<0.001$, compared to time 0 minutes by one-way ANOVA followed by Post-Hoc tests (B and C).

Fig.6 (A) Validation of shRNA-mediated knockdown of GPR43. Undifferentiated immortalized BAT (IM-BAT) cells were transfected with shRNA non-targeting control (#RHS6848) or shRNA targeting GPR43 (sh-GPR43-1: TRCN0000027581; sh-GPR43-2: TRCN0000027541; sh-GPR43-3: TRCN0000027562; sh-GPR43-4: TRCN0000027552). Following selection by puromycin, cells were lysed with Qiazol after 7 days of differentiation and subjected to real-time PCR analysis. Data are presented as mean ± S.E.M, with significant differences compared to mock control, **P<0.01, ***P<0.001 as analysed by one-way ANOVA followed by Post-Hoc tests. (B & C) IM-BATs transfected with non-targeting shRNA control or shRNA targeting GPR43 were treated with or without acetate during differentiation. Relative mRNA levels of UCP1 (B) and relative mitochondrial DNA (mtDNA) levels (C) were analysed by real-time PCR, where silencing the GPR43 receptor showed no change in UCP-1 or mtDNA expression. Data are presented as mean ± S.E.M.. *P <0.05 compared to no acetate treated controls by student's t-test. (D) Time-course of ERK and CREB activation following treatment with acetate in IM-BAT cells expressing GRP43 shRNA. Puromycin selected IM-BAT cells with GPR43 shRNA were differentiated for 5 days and either left untreated or treated with Acetate (10 mM) for 5, 10, 15, 30 and 60 minutes. Data are presented as mean ± S.E.M..

Fig.7 (A) Effects of U0126 on acetate-induced ERK and CREB phosphorylation. (B) Effects of pertussis toxin (PTX) on acetate-induced ERK and CREB phosphorylation. (C) Effects of Gallein on acetate-induced ERK and CREB phosphorylation. (D) Effects of U73122 on acetate-induced ERK and CREB phosphorylation. In all experiments, immortalized BAT (IM-BAT) cells were differentiated for 5 days and stimulated with acetate (10 mM) for 15 min after pre-treatment with U0126 (10 μM), PTX (1 μg ml^{-1}), Gallein (10 μM), or U73122 (1 μM) for 3h. Data are presented as mean ± S.E.M.. *P <0.05, **P<0.01, ***P<0.001 compared by one-way ANOVA followed by Post-Hoc tests.

Supplementary Figure 1

Identification of immortalized BAT (IM-BAT) cells as a brown adipocyte model *in vitro*. (A) Macroscopic pictures of Oil Red-O staining of immortalized BAT (IM-BAT) cells differentiated for 7 days. (B) Expression levels of UCP1 mRNA in the course of adipogenesis of IM-BAT cells. IM-BAT cells were differentiated and cell lysate were collected at day 0, day 3, day 6 and day 9. Transcription of UCP-1 was detected by real-time PCR. (C) UCP-1 and mitochondrial DNA levels in differentiated IM-BAT cells and differentiated 3T3-L1 cells. IM-BAT and 3T3-L1 cells were differentiated; total RNA and total DNA was isolated by GenElute™ Mammalian Total RNA Miniprep Kit and QIAamp DNA Mini kit, respectively. UCP-1 transcription and mitochondrial DNA to genomic DNA ratio were measured by real-time PCR. (D) Effects of CL-316,243 (CL) treatment on expression levels of UCP1 in differentiated IM-BAT cells. IM-BAT cells were differentiated then treated with CL-316,243 (10 μM) for 6 h. Expression of UCP1 was measured by real-time PCR. (E) Effects of CL-316,243 (CL) treatment on glucose uptake in differentiated IM-BAT cells. IM-BAT cells were differentiated and starved in glucose-free, serum-free DMEM:F12 medium for 3 h. The cells then were treated with CL-316,243 (10 μM) for 3 h and stained with 2-NBDG (150 μg/ml). Fluorescence (ex/em = 465/540 nm) was measured by flow cytometry. (F) Effects of insulin treatment on Akt activation in differentiated IM-BAT cells. IM-BAT cells were differentiated and serum-starved overnight. The cells then were treated with insulin (1 μM) for 15 min. The phosphorylated Akt and total Akt were measured by western blots. Data are presented as mean ± S.E.M.. *P <0.05, **P<0.01, ***P<0.001.

Supplementary Figure 2

Concentration-dependent effects of acetate treatment on PGC-1α and UCP1 during brown adipogenesis in immortalized BAT (IM-BAT) cells. IM-BAT cells were differentiated for 7 days with or without acetate at different concentrations (0.1 - 10 mM, from day 2 to day 7). The cells were lysed with QIAzol. The

transcription levels of PGC-1α, and UCP1 were measured by real-time PCR. Data are presented as mean ± S.E.M. *P<0.05, **P<0.01, ***P<0.001 compared to control by student's t-tests.

Supplementary Figure 3

The effect of acetate treatment during differentiation on the mitochondrial respiratory capacity in immortalized BAT (IM-BAT) cells in response to β-adrenergic stimulation. The x axis represents the applied XF24 protocol measurements and the vertical line indicates the time of addition of CL316,234 (CL). Data are expressed as the percentage of the basal value measured at the time point 3 (four replicates) in the control group. OCR: oxygen consumption rate.

Supplementary Figure 4

Relative mRNA levels of brown adipocyte markers in T37i cells treated with or without acetate during differentiation. Data are presented as mean ± S.E.M.. *P <0.05, **P<0.01 by student's t-test compared with no acetate treated controls.

Table.1 Primer sequence

Primer	Sequence (5'-3')
mGPR43-Forward	CCACTGTATGGAGTGATCGCTG
mGPR43-Reverse	GGGTGAAGTTCTCGTAGCAGGT
mBMP7-Forward	GGAGCGATTTGACAACGAGACC
mBMP7-Reverse	AGTGGTTGCTGGTGGCTGTGAT
mPRDM16-Forward	ATGCGAGGTCTGCCACAAGT
mPRDM16-Reverse	CTGCCAGGCGTGTAATGGTT
mPPARg-Forward	GGCTTCCACTATGGAGTTCA
mPPARg-Reverse	GATCCGGCAGTTAAGATCAC
mPGC1a-Forward	TGCAGCCAAGACTCTGTATG
mPGC1a-Reverse	ATTGGTCGCTACACCACTTC
mUCP1-Forward	CACTCAGGATTGGCCTCTAC
mUCP1-Reverse	CTGACCTTCACGACCTCTGT
mAP2-Forward	ATCACCGCAGACGACAGGAA
mAP2-Reverse	TTCCACCACCAGCTTGTCAC
mRPL19-Forward	GGAAAAAGAAGGTCTGGTT
mRPL19-Reverse	TGATCTGCTGACGGGAGT
m_mtDNA_D-loop_Forward	AATCTACCATCCTCCGTG
m_mtDNA_D-loop_Reverse	GACTAATGATTCTTCACCGT
m_18S_rDNA_Forward	CATTCGAACGTCTGCCCTATC
m_18S_rDNA_Reverse	CCTGCTGCCTTCCTTGGA

Figure 1

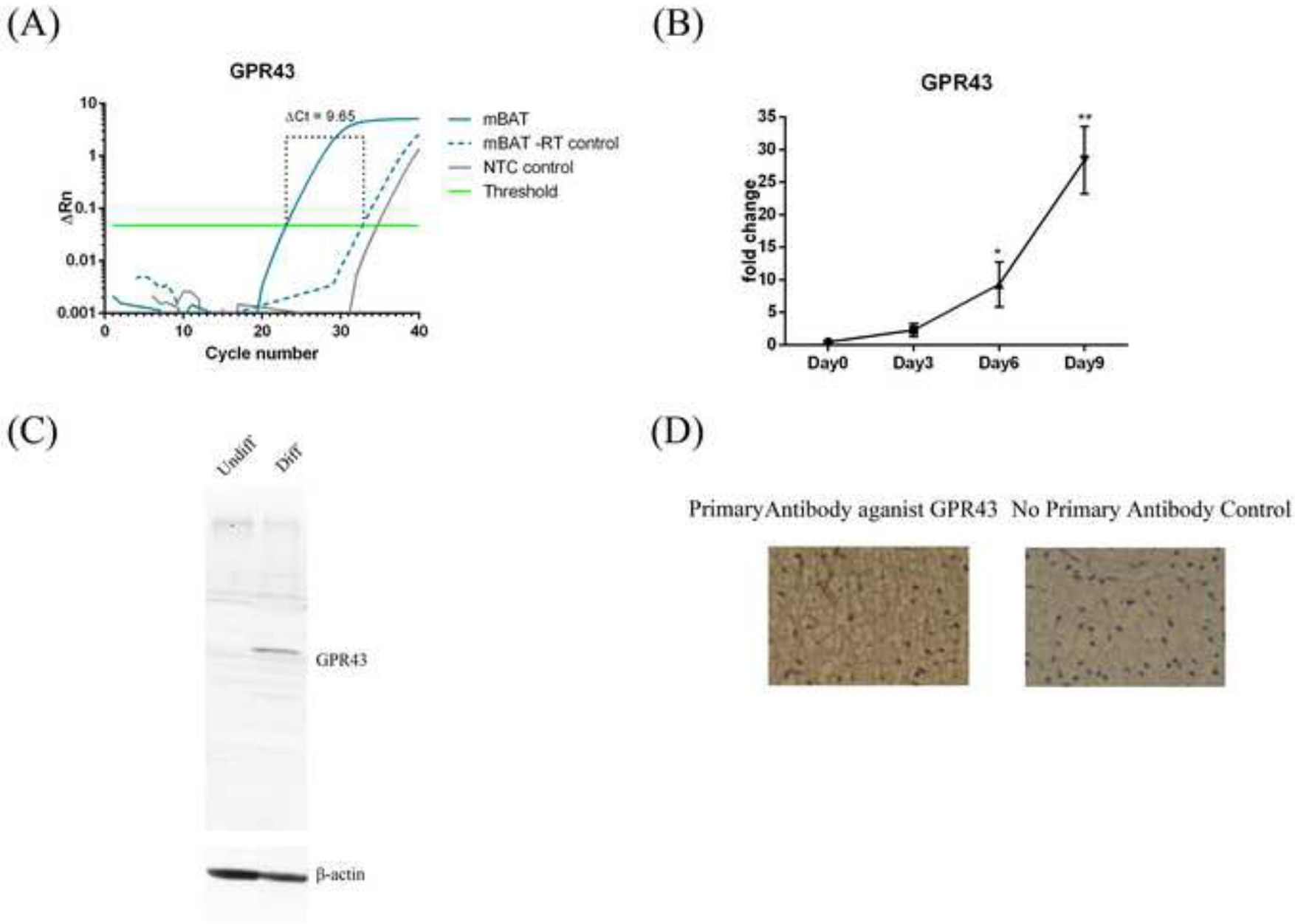
(A)
GPR43
ΔCt = 9.65
mBAT
mBAT -RT control
NTC control
Threshold
ΔRn
Cycle number
(B)
GPR43
fold change
Day0
Day3
Day6
Day9
(C)
Undiff
Diff
GPR43
β-actin
(D)
Primary Antibody aganist GPR43
No Primary Antibody Control

Figure 2

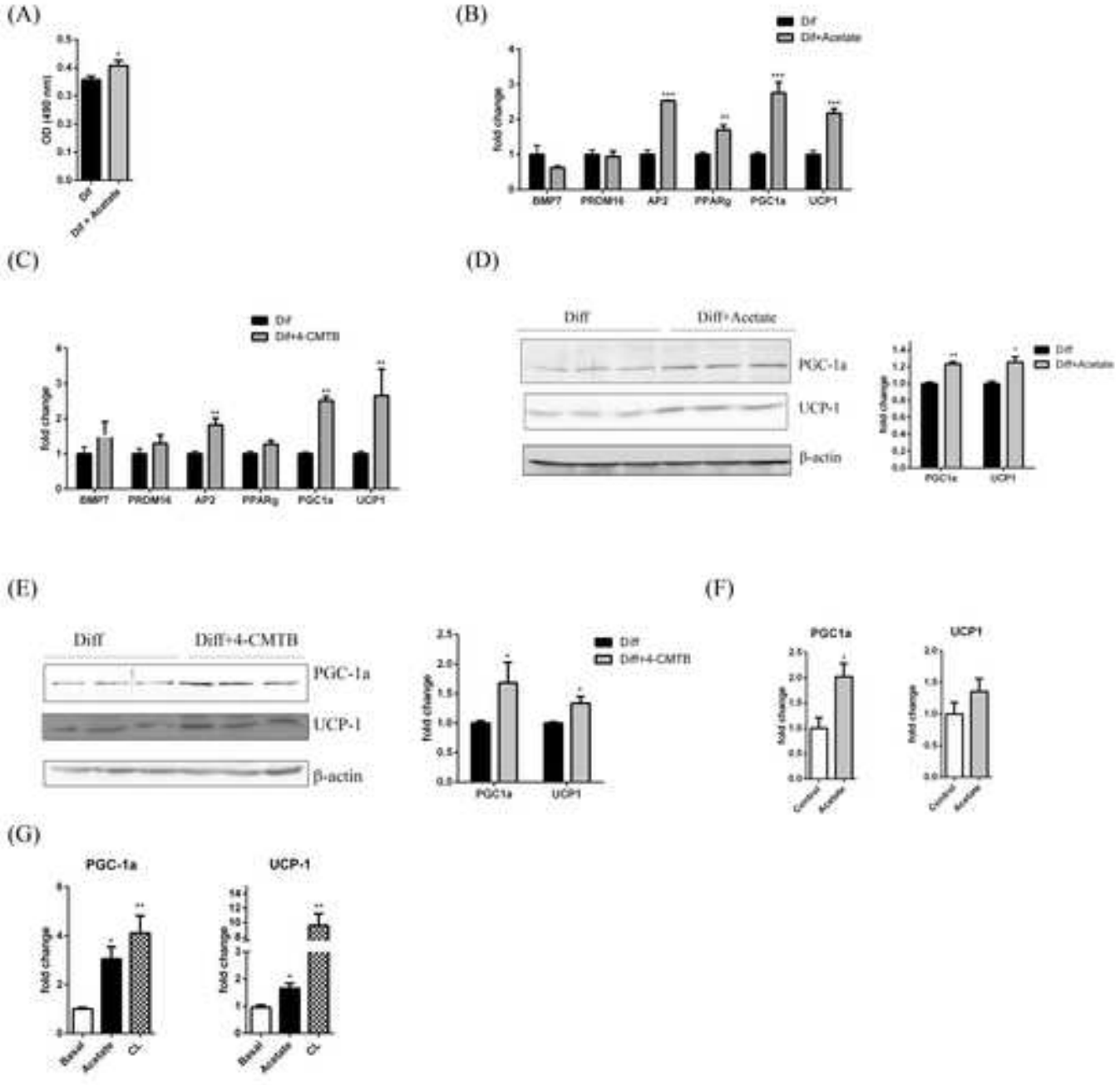
(A)
OD (490 nm)
Diff
Diff + Acetate
(B)
Diff
Diff+Acetate
fold change
BMP7
PRDM16
AP2
PPARg
PGC1a
UCP1
(C)
Diff
Diff+4-CMTB
fold change
BMP7
PRDM16
AP2
PPARg
PGC1a
UCP1
(D)
Diff
Diff+Acetate
PGC-1a
UCP-1
β-actin
fold change
PGC1a
UCP1
(E)
Diff
Diff+4-CMTB
PGC-1a
UCP-1
β-actin
Diff
Diff+4-CMTB
fold change
PGC1a
UCP1
(F)
PGC1a
UCP1
fold change
Control
Acetate
(G)
PGC-1a
UCP-1
fold change
Basal
Acetate
CL

Figure 3

(A)

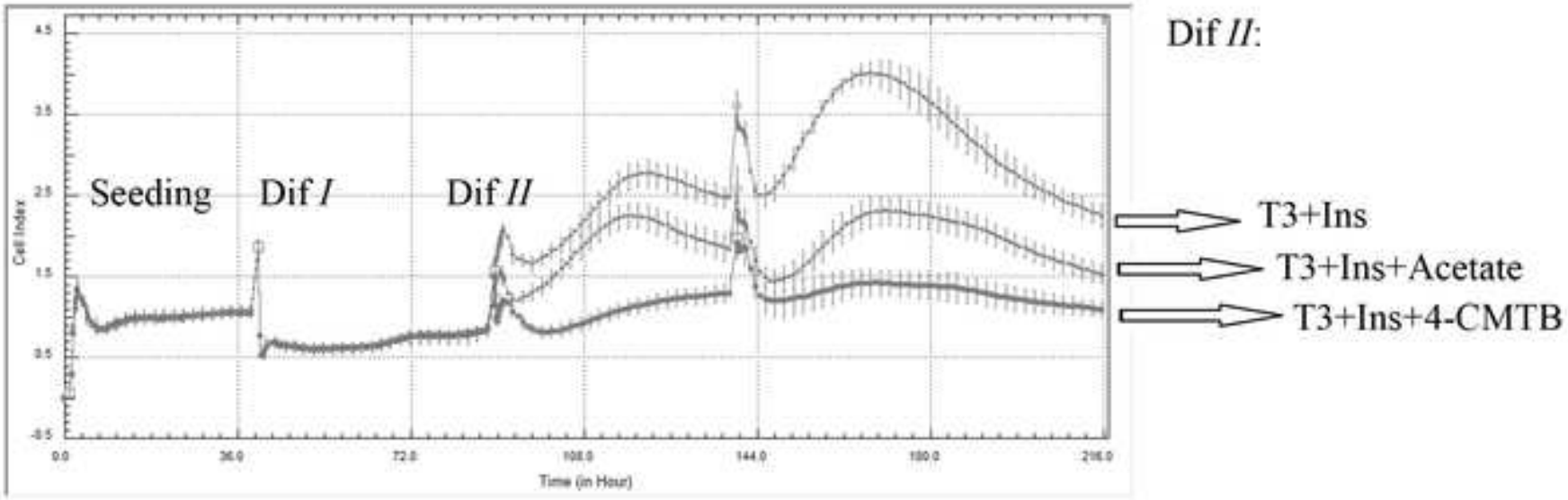
Seeding
Dif *I*
Dif *II*
Cell Index
Time (in Hour)
Dif *II*:
T3+Ins
T3+Ins+Acetate
T3+Ins+4-CMTB

(B)

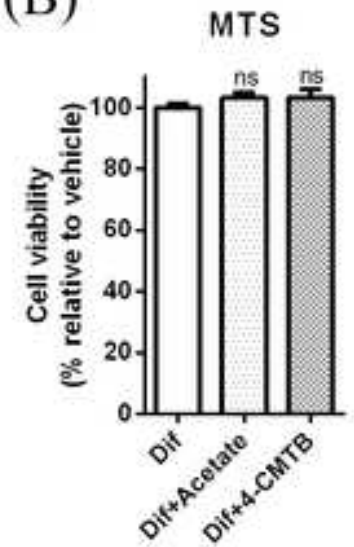
MTS
Cell viability
(% relative to vehicle)
ns
ns
100
80
60
40
20
0
Dif
Dif+Acetate
Dif+4-CMTB

Figure 4

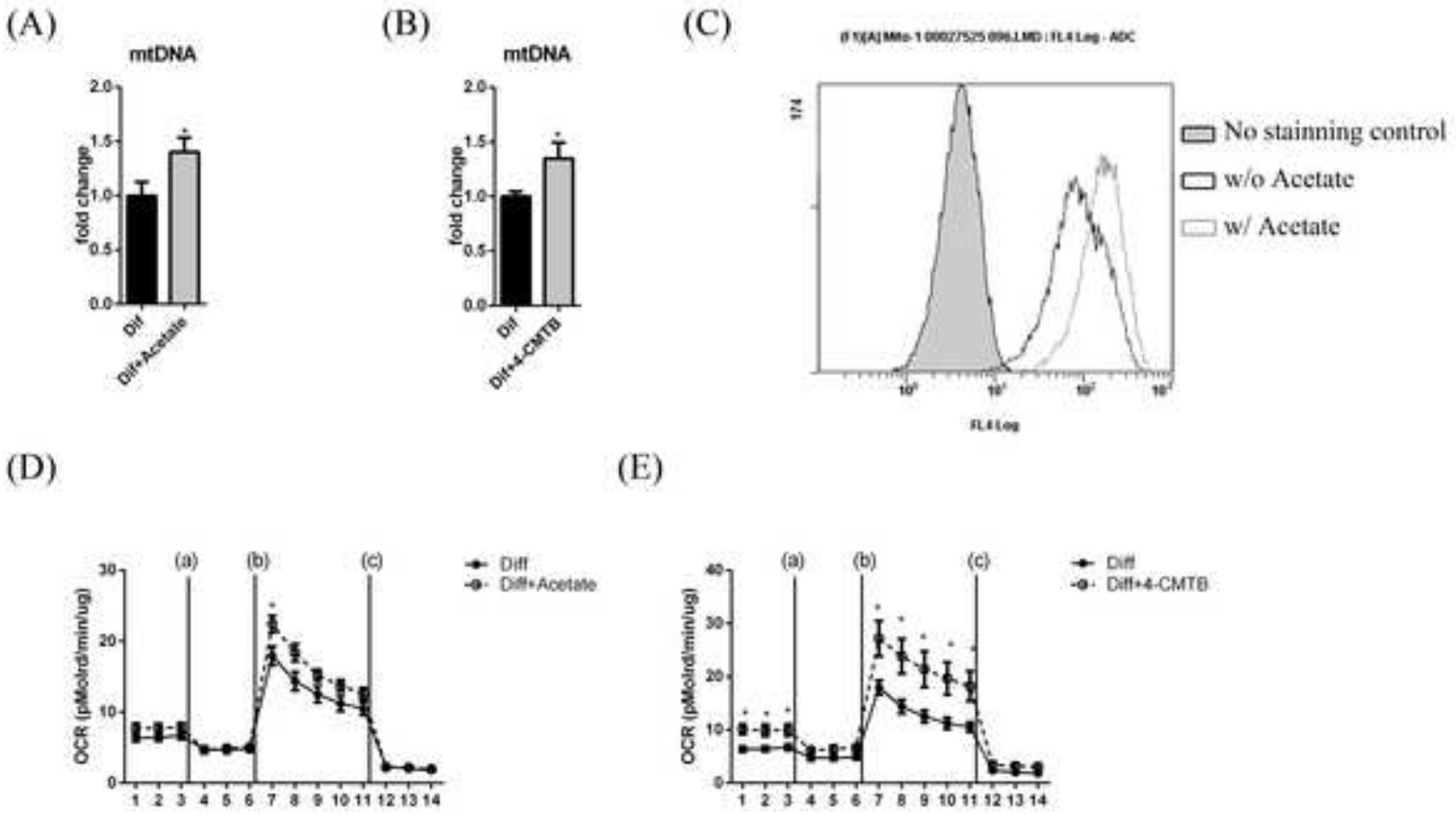
(A)
mtDNA
fold change
2.0
1.5
1.0
0.5
0.0
Dif
Dif+Acetate
(B)
mtDNA
fold change
2.0
1.5
1.0
0.5
0.0
Dif
Dif+4-CMTB
(C)
No stainning control
w/o Acetate
w/ Acetate
FL4 Log
(D)
OCR (pMol/rd/min/ug)
(a)
(b)
(c)
Diff
Diff+Acetate
1 2 3 4 5 6 7 8 9 10 11 12 13 14
(E)
OCR (pMol/rd/min/ug)
(a)
(b)
(c)
Diff
Diff+4-CMTB
1 2 3 4 5 6 7 8 9 10 11 12 13 14

Figure 5

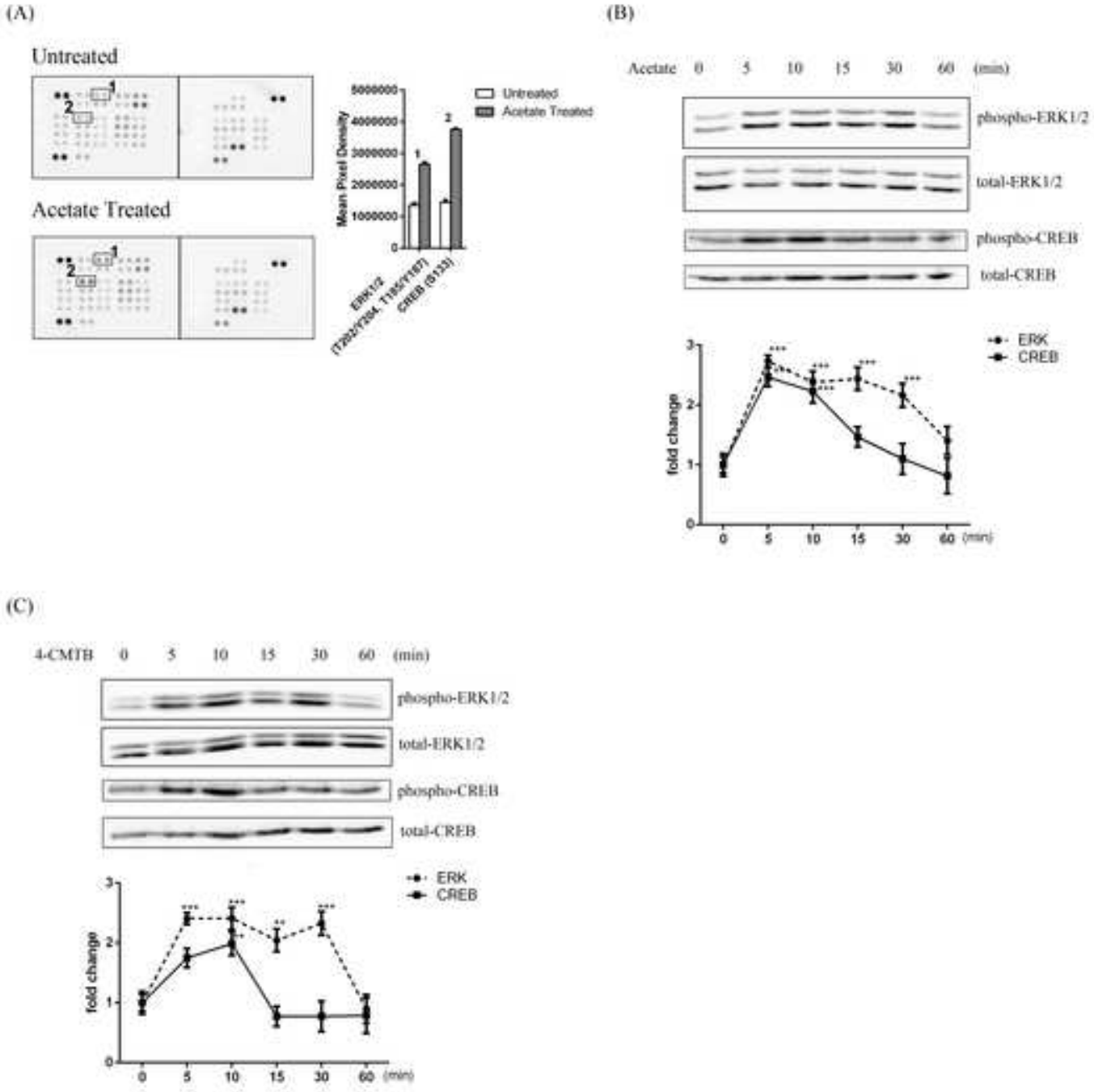
(A)
Untreated
Acetate Treated
Mean Pixel Density
Untreated
Acetate Treated
ERK1/2 (T202/Y204, T185/Y187)
CREB (S133)
(B)
Acetate 0 5 10 15 30 60 (min)
phospho-ERK1/2
total-ERK1/2
phospho-CREB
total-CREB
fold change
ERK
CREB
(C)
4-CMTB 0 5 10 15 30 60 (min)
phospho-ERK1/2
total-ERK1/2
phospho-CREB
total-CREB
fold change
ERK
CREB

Figure 6

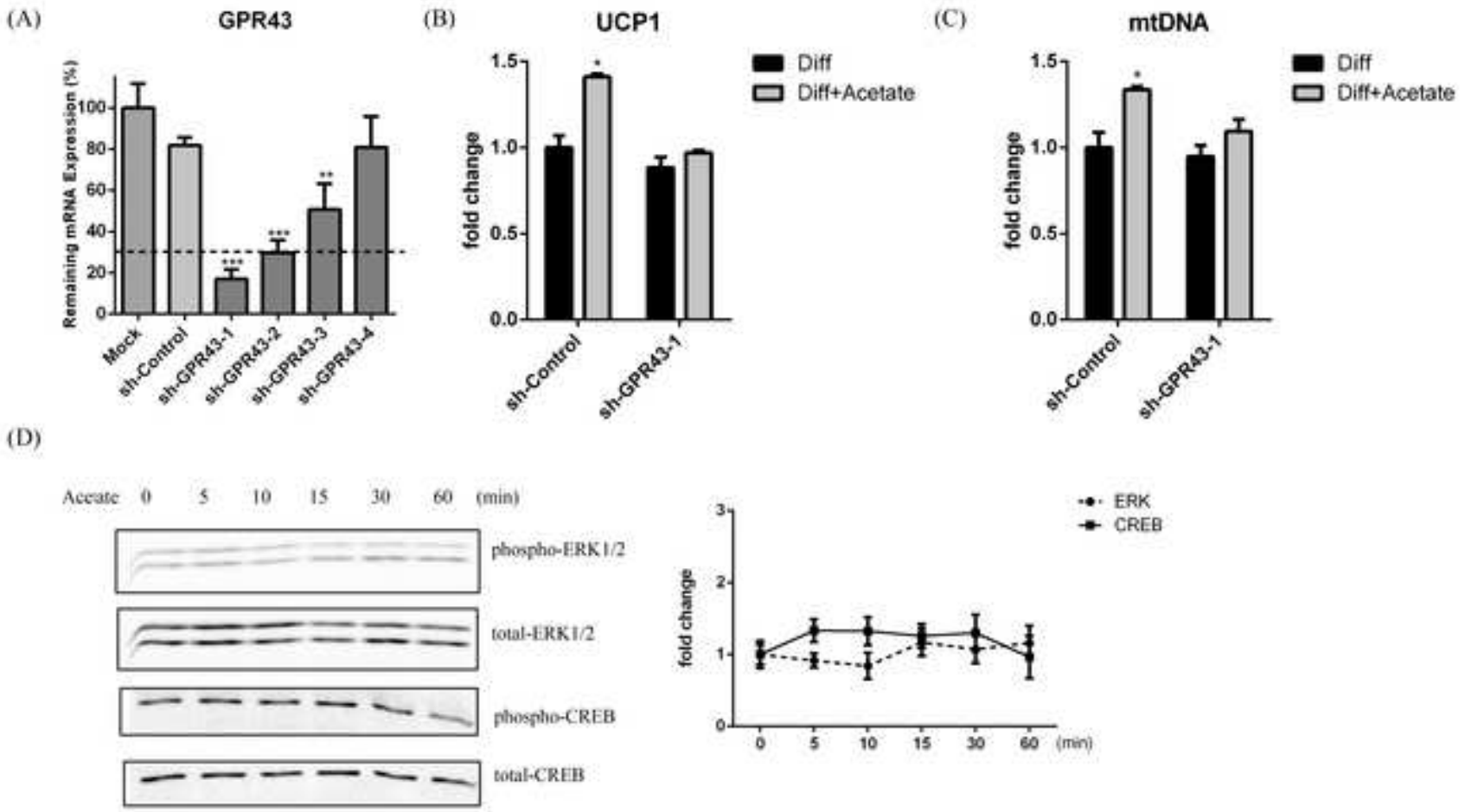
(A)
GPR43
Remaining mRNA Expression (%)
Mock
sh-Control
sh-GPR43-1
sh-GPR43-2
sh-GPR43-3
sh-GPR43-4
(B)
UCP1
fold change
Diff
Diff+Acetate
sh-Control
sh-GPR43-1
(C)
mtDNA
fold change
Diff
Diff+Acetate
sh-Control
sh-GPR43-1
(D)
Acetate 0 5 10 15 30 60 (min)
phospho-ERK1/2
total-ERK1/2
phospho-CREB
total-CREB
ERK
CREB
fold change
(min)

Figure 7

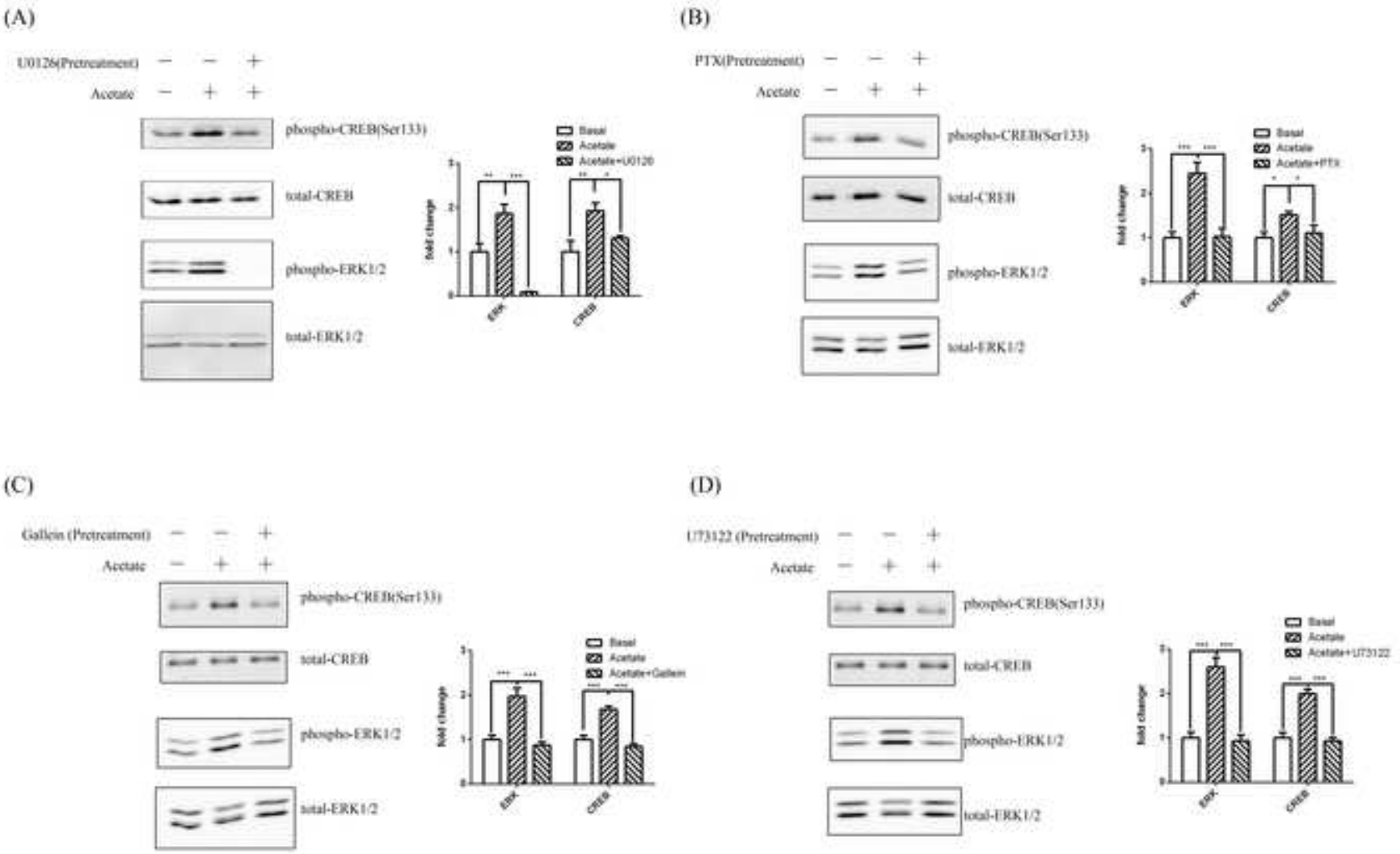
(A)
U0126(Pretreatment)
Acetate
phospho-CREB(Ser133)
total-CREB
phospho-ERK1/2
total-ERK1/2
Basal
Acetate
Acetate+U0126
fold change
ERK
CREB
(B)
PTX(Pretreatment)
Acetate
phospho-CREB(Ser133)
total-CREB
phospho-ERK1/2
total-ERK1/2
Basal
Acetate
Acetate+PTX
fold change
ERK
CREB
(C)
Gallein (Pretreatment)
Acetate
phospho-CREB(Ser133)
total-CREB
phospho-ERK1/2
total-ERK1/2
Basal
Acetate
Acetate+Gallein
fold change
ERK
CREB
(D)
U73122 (Pretreatment)
Acetate
phospho-CREB(Ser133)
total-CREB
phospho-ERK1/2
total-ERK1/2
Basal
Acetate
Acetate+U73122
fold change
ERK
CREB

Antibody Table

Peptide/protein target	Antigen sequence (if known)	Name of Antibody	Manufacturer, catalog #, and/or name of individual providing the antibody	Species raised in; monoclonal or polyclonal	Dilution used
phospho-Erk1/2 (Thr202/Tyr204)		Phospho-p44/42 MAPK (Erk1/2) (Thr202/Tyr204) Antibody #9101	Cell Signaling (#9101)	Rabbit, monoclonal	1:1500
Erk1/2		p44/42 MAPK (Erk1/2) (137F5) Rabbit mAb #4695	Cell Signaling (#4695)	Rabbit , monoclonal	1:2000
phospho-CREB (Ser133)		Phospho-CREB (Ser133) (87G3) Rabbit mAb #9198	Cell Signaling (#9198)	Rabbit , monoclonal	1:1000
CREB		CREB (48H2) Rabbit mAb #9197	Cell Signaling (#9197)	Rabbit , monoclonal	1:1000
UCP1		Anti-UCP-1 antibody	Sigma (U6382)	Rabbit, polyclonal	1:1000
PGC-1α		PGC-1 Antibody (H-300): sc-13067	Santa Cruz (sc-13067)	Rabbit, polyclonal	1:1000
β-Actin		β-Actin Antibody (C4): sc-47778	Santa Cruz (sc-47778)	Mouse, monoclonal	1:5000

Supplemental Figure 1

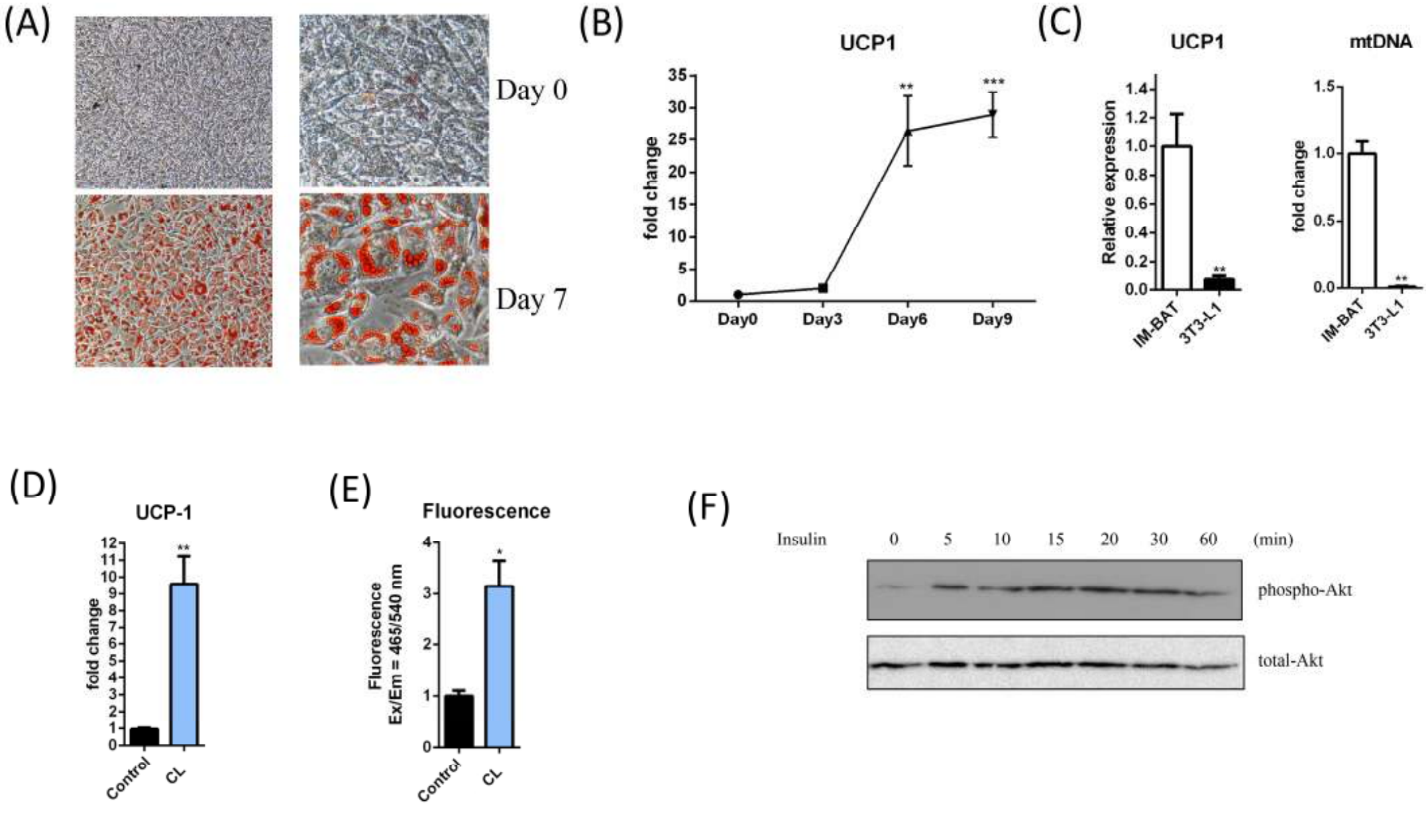

Supplemental Figure 2

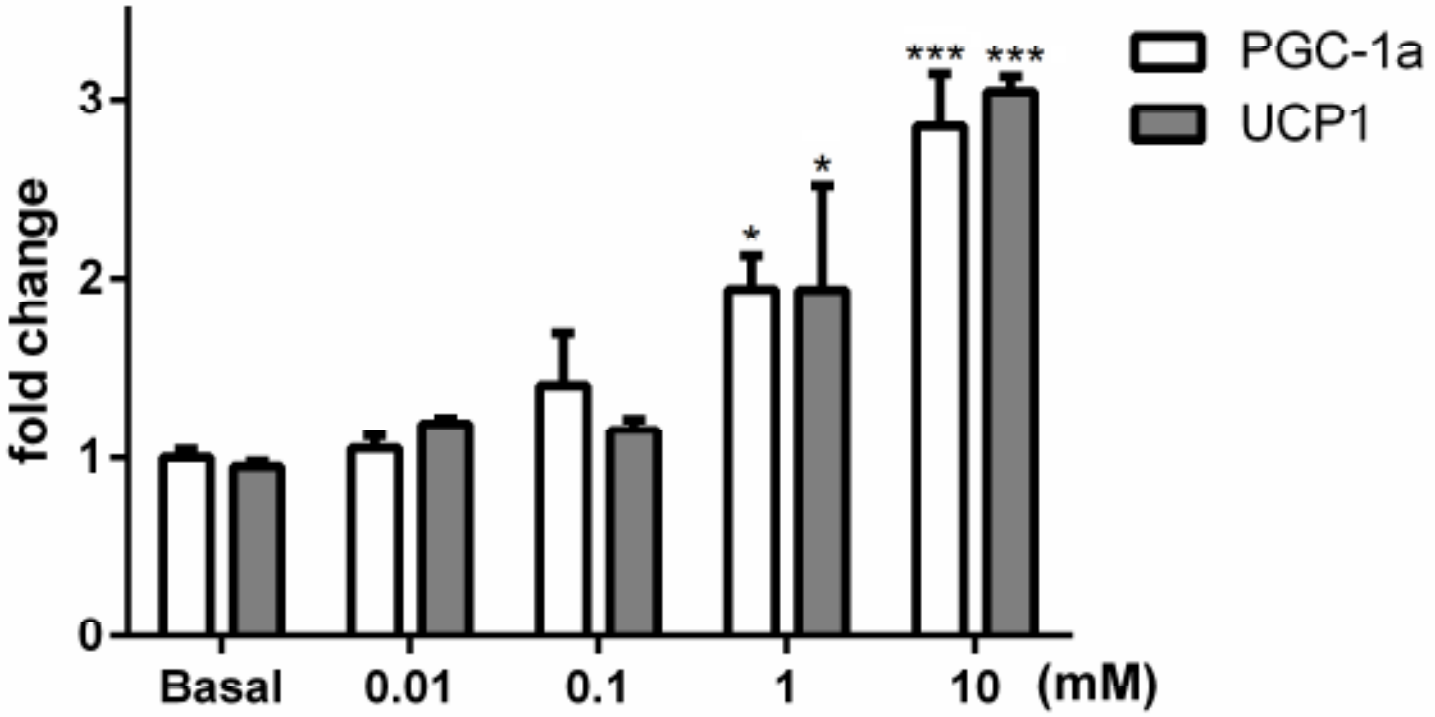

Supplemental Figure 3

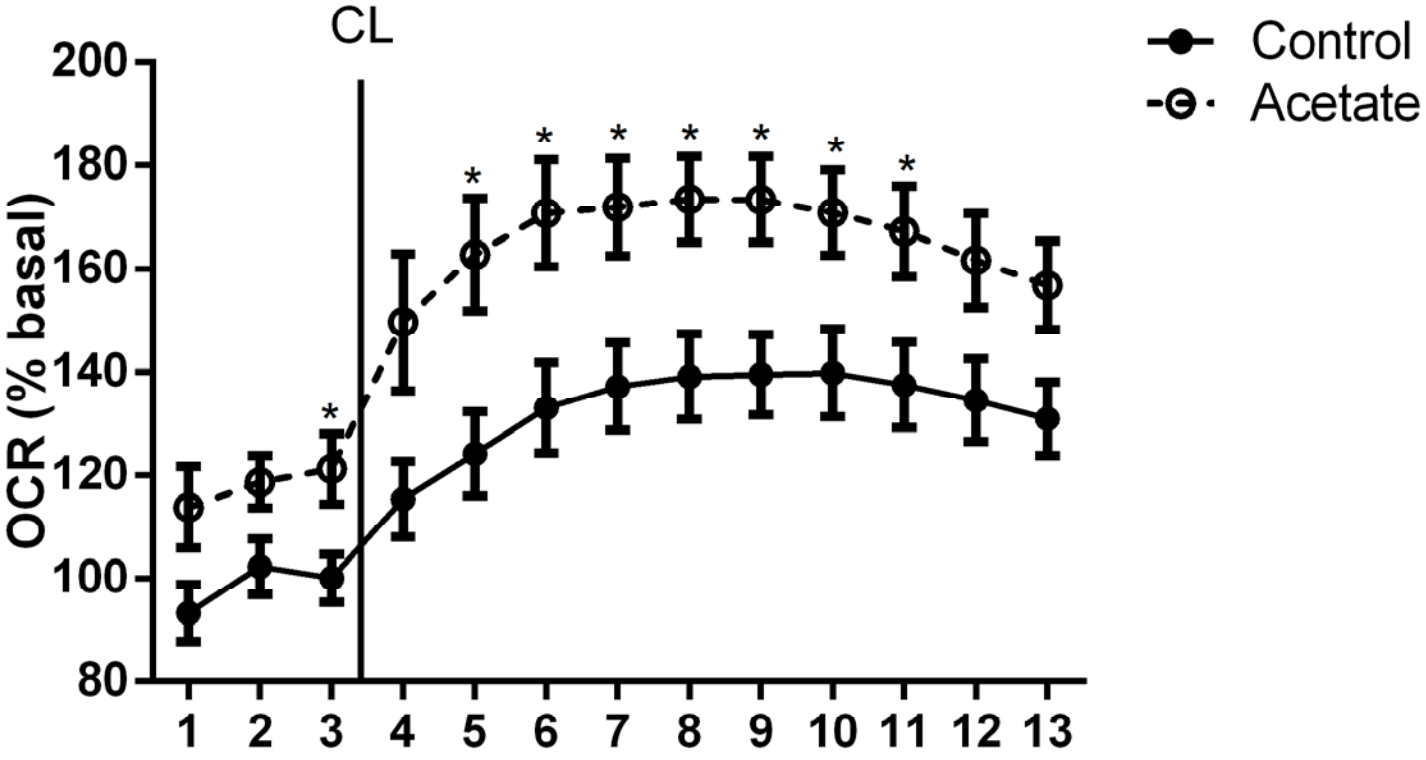

Supplemental Figure 4